

Distilling Spectral Graph for Object-Context Aware Open-Vocabulary Semantic Segmentation

Chanyoung Kim¹ Dayun Ju¹ Woojung Han¹ Ming-Hsuan Yang^{1,2} Seong Jae Hwang¹

¹Yonsei University ²University of California, Merced

Abstract

Open-Vocabulary Semantic Segmentation (OVSS) has advanced with recent vision-language models (VLMs), enabling segmentation beyond predefined categories through various learning schemes. Notably, training-free methods offer scalable, easily deployable solutions for handling unseen data, a key goal of OVSS. Yet, a critical issue persists: lack of object-level context consideration when segmenting complex objects in the challenging environment of OVSS based on arbitrary query prompts. This oversight limits models’ ability to group semantically consistent elements within object and map them precisely to user-defined arbitrary classes. In this work, we introduce a novel approach that overcomes this limitation by incorporating object-level contextual knowledge within images. Specifically, our model enhances intra-object consistency by distilling spectral-driven features from vision foundation models into the attention mechanism of the visual encoder, enabling semantically coherent components to form a single object mask. Additionally, we refine the text embeddings with zero-shot object presence likelihood to ensure accurate alignment with the specific objects represented in the images. By leveraging object-level contextual knowledge, our proposed approach achieves state-of-the-art performance with strong generalizability across diverse datasets.

1. Introduction

Open-vocabulary semantic segmentation (OVSS) [9, 28, 49, 50, 53] aims to predict pixel-level labels for *arbitrary prompts* defined by user input (e.g., the proper noun `Space Needle` in Fig. 1(a)), advancing beyond previous models scoped to predefined static classes [10, 18, 35]. To achieve this, fully supervised OVSS models [11, 48, 51] enhance generalization to seen classes using labeled training data. Yet, their reliance on seen classes during training may risk overfitting and limit scalability, as labeled data is required for retraining to adapt to new domains [38].

Project Page: <https://micv-yonsei.github.io/cass/>

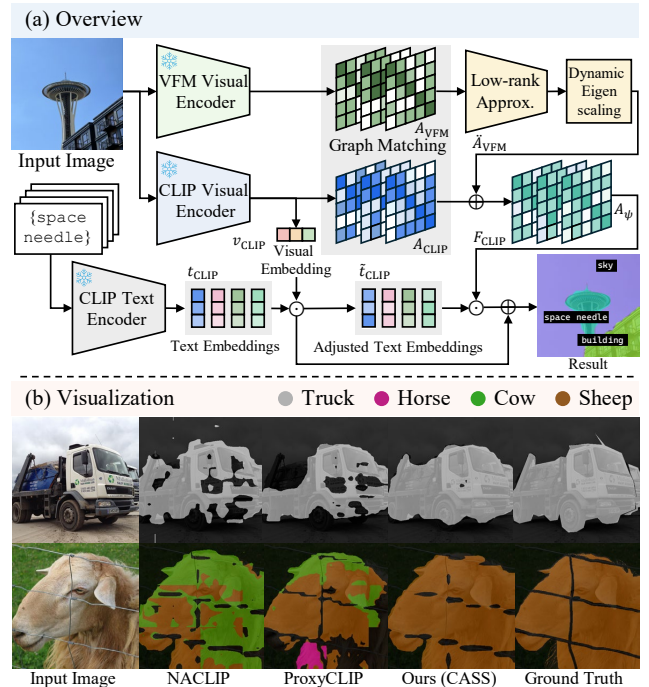


Figure 1. We present CASS, object-level Context-Aware training-free open-vocabulary Semantic Segmentation model. (a) *Overview*: Our method distills the vision foundation model’s (VFM) object-level contextual spectral graph into CLIP’s attention and refines query text embeddings towards object-specific semantics. (b) *Object-Level Context*: This result illustrates how incorporating object-level context improves segmentation accuracy by unifying object-wise components into a user-defined object class; for example, (top row) our approach precisely segments the truck’s body, wheels, and cargo area and (bottom row) accurately groups elements into a single object, such as the sheep, whereas base-lines [16, 25] often fail to achieve this unified segmentation.

To better address this, recent studies [16, 24, 25, 43, 53] propose training-free OVSS methods that leverage pre-trained vision-language models (VLMs) (e.g., CLIP [34]) to integrate aligned visual and textual representations. These works focus on improving semantic association between visual patches in CLIP image encoder to produce more

precise segmentation maps, achieving highly promising results. This training-free scheme offers key advantages: it (1) generalizes well to unseen classes without requiring additional labeled data, making it more scalable, thus (2) allows direct adaptation to dynamic real-world applications. Capitalizing on these benefits, training-free OVSS aligns with OVSS’s core goal of adaptability across diverse domains, enabling it to reach its full potential.

We tackle OVSS in a *training-free* manner, presenting a challenging and practical approach aligned with OVSS’s true objectives. Although existing training-free methods [20, 25, 42, 43] perform well on numerous tasks, they all share a common limitation: the lack of “*object-level context*.” To understand “*object-level context*”, consider a truck and sheep in Fig. 1(b). Components comprising a truck, such as its wheels and cargo area, should be grouped as a single entity. Similarly, components of a sheep should be accurately unified under the correct user-given object class. However, existing training-free OVSS methods, which use CLIP as the image backbone for segmentation, often struggle to capture object-level context, failing to group object components into a single, user-defined object. These challenges stem from CLIP’s focus on learning global image semantics, which may be insufficient for capturing dense object-level semantics [16, 43, 53]. Thus, to achieve accurate training-free OVSS, a proper object-level context must be considered in CLIP.

We address the challenges of training-free OVSS by introducing the object-level context and propose the Context-Aware Semantic Segmentation (CASS) model. Vision foundation models (VFMs), such as DINO [8, 33], capture fine-grained, patch-level semantics but lack object-level context, making them unsuitable for direct use in tasks requiring such context. Recent studies [21, 31] have shown that applying graph spectral techniques to VFM attention graphs can transform patch-level representations into object-level representations. Accordingly, we apply spectral techniques to extract essential object-level context from the VFM attention graph. The extracted spectral features can be used directly for segmentation (e.g., clustering eigenvectors); however, this approach may not be suitable for OVSS, where textual alignment is essential. Thus, we propose distilling low-rank components of VFM into CLIP to enhance its object-level context understanding, while maintaining alignment with textual information. Specifically, we decompose the VFM’s attention graph to extract low-rank components, filtering irrelevant information while emphasizing essential object-level context. These low-rank components are then distilled into CLIP’s attention to embed the fundamental object structure of the VFM graph.

Our model also leverages CLIP’s highly effective zero-shot object classification capability (i.e., object presence prior), widely validated in prior work [19, 29, 34], to cap-

ture detailed object-level context within scenes. As such, we adjust the text embeddings based on the object presence prior encoded by CLIP. This process involves refining the embeddings to better align with object-specific semantics. Then, we refine patch-text similarities using the object presence prior, ensuring that the final segmentation map reflects an object-specific perspective. Our CASS, carefully designed to enhance object-level contextual knowledge, captures richer intra-object coherence and enables cohesive groupings of semantically related elements.

The main contributions of this work are:

- We enhance object-level context by distilling rich semantic understanding from VFM into the CLIP attention mechanism, facilitating a more consistent grouping of each object into a unified semantic entity.
- We present object presence prior-driven text embeddings and patch-text similarity refinement, promoting the model to precisely classify objects.
- We demonstrate the performance of our model in various semantic segmentation datasets and achieve state-of-the-art performance in training-free OVSS.

2. Related Works

Open-Vocabulary Semantic Segmentation. Open-vocabulary semantic segmentation (OVSS) aims to segment images corresponding to arbitrary user-given prompts, using vision-language aligned representations (e.g., CLIP [34]). Meanwhile, training-free approaches [3, 4, 25, 53] have risen for their ability to adapt directly to new tasks without extra training. Among these, methods [16, 25, 43, 53] that do not rely on additional datasets have gained attention, as they require no extra adaptation effort, aligning better with the objective of OVSS. Earlier approaches investigated leveraging CLIP features for better localization [26, 53] or for grounding proposed masks [20, 42]. SCLIP [43] uses correlative self-attention to improve inter-patch correlations. NA-CLIP [16] applies a Gaussian kernel to attention maps for better spatial consistency, and ProxyCLIP [25] integrates patch-wise consistent features from DINO [8]. Although these methods demonstrated strong results, they often struggle to group different parts of the same object due to a lack of explicit dense label knowledge. To this end, we attribute the underlying challenges of training-free OVSS by enriching the object-level contextual understanding.

Vision Foundation Models. Vision Foundation Models (VFMs), especially vision transformer (ViT)-based [14] self-supervised models (e.g., DINO [8, 33]), have significantly advanced computer vision through their ability to capture patch-wise semantic understanding at both the feature and attention levels. Among various downstream tasks [17, 30, 37, 41, 44] leveraging VFM’s capability, one line of research focuses on leveraging the attention com-

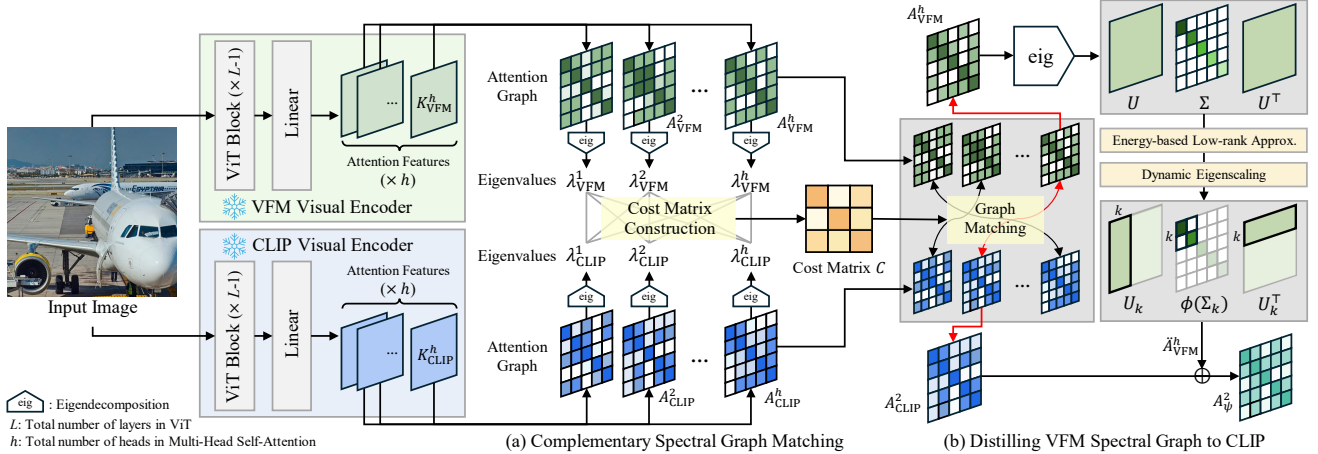


Figure 2. Detailed illustration of our proposed *training-free* spectral object-level context distillation mechanism in Sec. 3.2. By matching the attention graphs of VFM and CLIP head-by-head to establish complementary relationships, and distilling the fundamental object-level context of the VFM graph to CLIP, we enhance CLIP’s ability to capture intra-object contextual coherence.

ponents in VFM [21, 31, 41], which exhibit a detailed understanding of patch-wise semantic interaction between different image regions. Thus, while ProxyCLIP [25] utilizes VFM features, our method takes a different effort by treating the attention mechanism in VFM as a graph. We then extract core structural patterns of the VFM graph to emphasize object-level context, providing an effective solution for producing precise object masks in training-free OVSS.

Object-Level Semantic Segmentation. Semantic segmentation groups object components that have similar semantics into a single mask, traditionally achieved through models trained on extensive human-labeled, pixel-wise annotations [10, 18, 35]. However, despite recent advancements in unsupervised semantic segmentation [17, 37] (USS) that do not rely on dense labels, a core challenge persists: individual object components are not consistently grouped into a single entity. To address this issue, recent USS studies [21, 36, 45] have incorporated object-level representation learning to improve the model’s ability to merge single objects into unified entities. However, these efforts have not been considered in the training-free OVSS task, which faces similar challenges in an unsupervised context. Therefore, we focus on enriching object-level context in training-free OVSS to achieve a more effective grouping of components within each object, enabling clearer and more consistent segmentation across diverse visual domains.

3. Method

We detail our proposed model, CASS, implemented in a training-free manner, as outlined in Fig 1(a). Our model jointly enhances object-level contextual understanding with two primary aspects: (1) Spectral Object-Level Context Distillation (Sec. 3.2) and (2) Object Presence-Driven Object-Level Context (Sec. 3.3). We first outline the basic pipeline of training-free OVSS in Sec. 3.1.

3.1. Preliminaries

CLIP Visual Encoder. Training-free OVSS models [16, 25, 43] leverage CLIP [34] for its rich alignment of visual and linguistic information. However, the CLIP ViT visual encoder $\mathcal{F}_{\text{CLIP}}^v$ focuses on aligning the [CLS] token with text embeddings during training, often neglecting the patch-wise spatial interactions among visual tokens that are crucial for dense prediction [16, 39, 43]. To produce CLIP feature representations more suitable for semantic segmentation tasks, we remove residual connection, feed-forward network, and self-attention layer in the final layer of $\mathcal{F}_{\text{CLIP}}^v$, following recent works [16, 43]. Specifically, when the set of visual tokens $Z = \text{Concat}[z_1, \dots, z_N] \in \mathbb{R}^{N \times D_z}$, where N is the total number of patches except [CLS] token and D_z denotes patch dimension space, is input into the final block of the ViT, the following operations are as

$$Z^* = \text{SA}(\text{LN}(Z)), \quad (1)$$

where SA and LN represent Self-Attention and Layer Normalization, respectively. The modified SA layer is

$$M_{\text{CLIP}}^i = \text{softmax}\left(A_{\text{CLIP}}^i / \sqrt{D_h}\right), \quad (2)$$

$$Z^* = \text{Concat}\left[M_{\text{CLIP}}^1 V_{\text{CLIP}}^1, \dots, M_{\text{CLIP}}^h V_{\text{CLIP}}^h\right] W^O, \quad (3)$$

where D_h denotes the head dimension, h is the number of heads, and $W^O \in \mathbb{R}^{D_z \times D_z}$ is the output projection matrix. We define CLIP attention map for i -th head as $A_{\text{CLIP}}^i = K_{\text{CLIP}}^i K_{\text{CLIP}}^{i\top} \in \mathbb{R}^{N \times N}$, where attention key $K_{\text{CLIP}} \in \mathbb{R}^{N \times D_h \times h}$ and value $V_{\text{CLIP}} \in \mathbb{R}^{N \times D_h \times h}$ result from the linear transformation of $\text{LN}(Z)$.

Inference Pipeline. We use a sliding window inference to ensure that ViT can capture detailed parts of the image by dividing the entire image \mathcal{I} into smaller windows $\hat{\mathcal{I}}$. The visual tokens $Z^* \in \mathbb{R}^{N \times D_z}$ are then computed from each $\hat{\mathcal{I}}$ through $\mathcal{F}_{\text{CLIP}}^v$ as in Eq. (1). To perform OVSS with

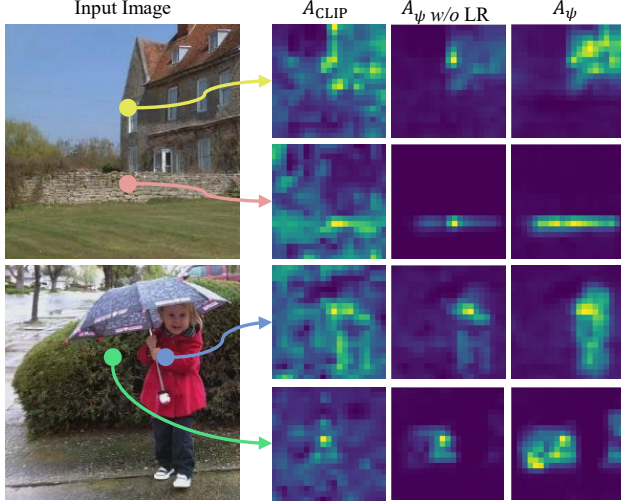


Figure 3. Attention score visualization for various query points. Left: Vanilla CLIP (A_{CLIP}) shows noisy, unfocused attention. Center: VFM-to-CLIP distillation *without* low-rank eigenscaling shows partial object grouping with limited detail. Right: Incorporating our low-rank eigenscaling (Eq. (7)) captures object-level context, improving grouping within a single object.

given texts, we project the visual tokens Z^* into the vision-language latent space as $F_{\text{CLIP}} = \mathcal{P}_{\text{CLIP}}(Z^*) \in \mathbb{R}^{N \times d}$, where $\mathcal{P}_{\text{CLIP}}$ is a projection matrix into CLIP latent space and d is the CLIP latent dimension. We compute patch-text similarity $\hat{S} \in \mathbb{R}^{N \times C}$ for each image window \hat{I} as

$$\hat{S} = F_{\text{CLIP}} \left[\{t_{\text{CLIP}}^i\}_{i=1}^C \right]^\top, \quad (4)$$

where $\{t_{\text{CLIP}}^i\}_{i=1}^C := \text{Concat} [t_{\text{CLIP}}^1, \dots, t_{\text{CLIP}}^C] \in \mathbb{R}^{C \times d}$ denotes the encoded text embeddings, and C is the number of classes. Finally, the results of all windows are combined to create a segmentation map for the entire image.

3.2. Spectral Object-Level Context Distillation

Our model CASS aims to capture such object-level contextual interaction within the image features to associate different parts of the same object. However, the limited ability of CLIP to capture semantic relationships between patches often neglects the object-level context, as illustrated in the left column of Fig. 3 (A_{CLIP}). To address this limitation, we leverage VFM (e.g., DINO [8]), enabling a deeper object-level contextual understanding. Among VFM features, we utilize VFM attention key component $K_{\text{VFM}} \in \mathbb{R}^{h \times N \times D_h}$. Specifically, we treat the VFM attention adjacency $A_{\text{VFM}} = K_{\text{VFM}} K_{\text{VFM}}^\top \in \mathbb{R}^{h \times N \times N}$ as a graph, where h represents the number of heads, and transfer crucial graph patterns from A_{VFM} to A_{CLIP} . However, a key question remains: ‘‘How do we account for the *multi-head attention mechanisms* in both VFM and CLIP?’’ In other words, ‘‘how do we match i -th VFM attention head A_{VFM}^i with j -th CLIP attention head A_{CLIP}^j ?’’ A straightforward approach is to distill the atten-

tion heads sequentially (i.e., $i = j$). Nevertheless, recent studies [27, 54] indicate that different attention heads focus on separate parts of the image. Thus, matching the optimal heads between VFM and CLIP is essential for precise attention distillation.

3.2.1. Complementary Spectral Graph Matching

We match graphs with *contrasting structures*, as shown in Fig 4, enabling VFM to supplement the object-level contextual knowledge that CLIP alone struggles to capture. To match an optimal head-wise attention graph, we exploit the spectral field of both A_{VFM} and A_{CLIP} . Our graph-matching mechanism has two main steps as illustrated in Fig. 2(a): (I) examining the eigenvalues of each graph and (II) matching optimal graph pairs using the spectral distribution.

(I) Eigenvalue Examination. For each graph from VFM and CLIP, denoted as A_{VFM}^i and A_{CLIP}^j for $(i = 1, \dots, h)$, we perform eigendecomposition. This yields the eigenvalues for each head h , λ_{VFM}^i and λ_{CLIP}^j , from which the top m fixed eigenvalues are selected. These eigenvalues contain each graph’s unique structural features, key properties essential for distinguishing different attention graph patterns.

(II) Graph Matching via Spectral Distribution. After obtaining eigenvalues for each head, we compute spectral distances to quantify structural differences, creating a cost matrix $\mathcal{C} \in \mathbb{R}^{h \times h}$ for each graph pair from VFM and CLIP:

$$\mathcal{C}_{ij} = 1 - \mathcal{D}_W(\bar{\lambda}_{\text{VFM}}^i, \bar{\lambda}_{\text{CLIP}}^j), \quad \forall i, j \in \{1, \dots, h\} \quad (5)$$

where $\bar{\lambda}_{\text{VFM}}^i$ and $\bar{\lambda}_{\text{CLIP}}^j$ represent the normalized eigenvalues of the i -th head of VFM and the j -th head of CLIP, respectively, and \mathcal{D}_W denotes the Wasserstein distance. Here, the Wasserstein distance is computed as $\mathcal{D}_W(u, v) = \sum_{i=1}^h |\text{sort}(u)_i - \text{sort}(v)_i|$, where u and v are the two input distributions, and the sort function orders the values of u and v in ascending order. After computing \mathcal{C} , we apply the Hungarian matching algorithm [23] to the cost matrix to find the optimal pairing of graph heads. This approach pairs graphs with contrasting characteristics, enabling complementary distillation of object-level context knowledge from A_{VFM} to A_{CLIP} , as described in the following section.

3.2.2. Distilling VFM Spectral Graph to CLIP

Once we match optimal graph pairs, we distill the VFM graph to CLIP (see Fig. 2(b)). For the sake of explanation, we assume that the i -th VFM attention head A_{VFM}^i is matched with the j -th CLIP attention head A_{CLIP}^j . An intuitive approach would be simply aggregating A_{VFM}^i and A_{CLIP}^j without any transformation. However, as shown in Fig. 3 ($A_{\psi \text{ w/o LR}}$), this approach may transfer noise or irrelevant information, highlighting the need to extract features that emphasize object-level context. From this realization, we leverage the low-rank components of VFM, which contain distinct object patterns within the graph structure [12].

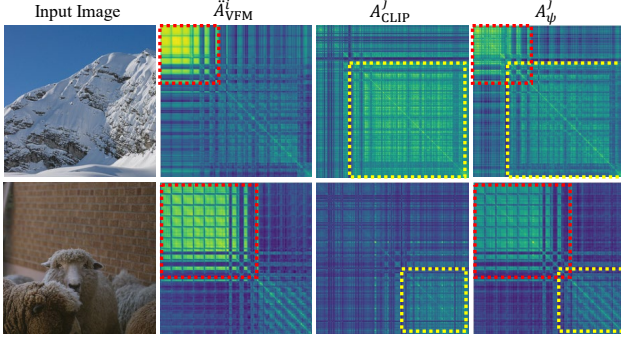


Figure 4. Visualization of the matched complementary graph pairs. The red dotted line indicates the focus areas of VFM, while the yellow dotted line highlights those for CLIP. By aggregating graphs with contrasting structural properties, we enhance the object-level context in A_{CLIP} supported by \hat{A}_{VFM} , resulting A_{ψ} .

Specifically, we (I) extract the critical object-level contextual structure of A_{VFM}^i via low-rank approximation and enhance the graph structure by dynamically scaling eigenvalues. Then, we (II) distill the approximated VFM graph into CLIP by aggregating graphs based on spectral distance.

(I) Low-Rank Dynamic Eigenscaling. Our goal is to transfer the essential object-level contextual structure of VFM graph A_{VFM} to CLIP. To achieve this, we extract low-rank components of the VFM graph using standard eigendecomposition, as $A_{\text{VFM}}^i = U\Sigma U^\top$, where U and Σ represent the eigenvector and the diagonal eigenvalue matrix, respectively. In the decomposed eigenbasis, we identify key object-level features of each graph by searching an optimal number of eigenvalues k through an energy-based approach. This ensures that the chosen k eigenvalues capture a significant portion of the graph’s energy, retaining essential structural information while discarding noise and less relevant details. More details on searching k can be found in the supplementary material. This process yields a low-rank approximated VFM graph, expressed as $\hat{A}_{\text{VFM}}^i = U_k \Sigma_k U_k^\top$.

We refine the low-rank components with a scaling function ϕ , which dynamically amplifies larger eigenvalues and reduces smaller ones. Compared to the conventional shrinkage function [2, 5], which only focuses on noise cutoff, our approach emphasizes essential structural information, particularly object-level context features, while suppressing noise and irrelevant details. More details on dynamic eigenscaling can be found in the supplementary material. The graph after applying dynamic eigenscaling is as

$$\hat{A}_{\text{VFM}}^i = U_k \phi(\Sigma_k) U_k^\top. \quad (6)$$

(II) VFM Graph Distillation. We distill the essential object-level contextual knowledge from the tailored VFM graph \hat{A}_{VFM}^i into the A_{CLIP}^j by aggregating their structures:

$$A_{\psi}^j = (w_{ij} \hat{A}_{\text{VFM}}^i + A_{\text{CLIP}}^j) / (w_{ij} + 1), \quad (7)$$

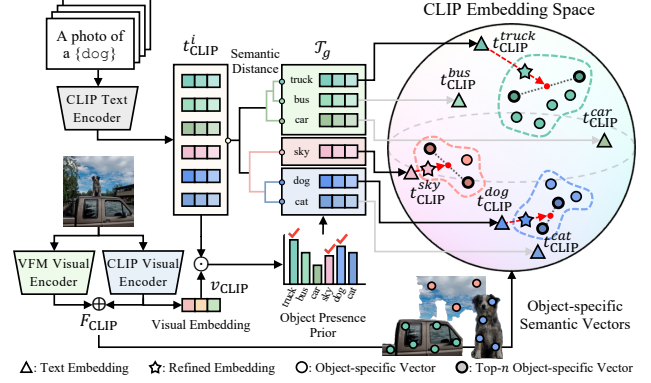


Figure 5. Detailed illustration of our object presence prior-guided text embedding adjustment module. The CLIP text encoder generates text embeddings for each object class, and the object presence prior is derived from both visual and text embeddings. Within hierarchically defined class groups, text embeddings are selected based on object presence prior, then refined in an object-specific direction to align with components likely present in the image.

where w_{ij} is defined as the Wasserstein distance between eigenvalues from both graphs as $\mathcal{D}_W(\bar{\lambda}_{\text{VFM}}^i, \bar{\lambda}_{\text{CLIP}}^j)$. This adaptively assigns higher weights to graphs with complementary structures, while reducing influence on those with similar structures. Our distillation strategy effectively transfers the critical object-level context from VFM to CLIP, ensuring multiple components of the same object are grouped into a unified semantic as illustrated in Fig. 3 (A_{ψ}). Therefore, we use A_{ψ} as our attention matrix instead of A_{CLIP} in Eq. (2) to compute the final visual feature F_{CLIP} .

3.3. Object Presence-Driven Object-Level Context

The spectral object-level context distillation in Sec. 3.2 enables precise object mask generation. However, due to the nature of OVSS, where users can provide arbitrary query prompts, different parts of the same object may still be assigned to closely related categories. Meanwhile, numerous studies [19, 29, 34] have demonstrated that CLIP excels in zero-shot object classification capability. Accordingly, we utilize the zero-shot object classification score encoded by CLIP (i.e., the object presence prior) to refine text embeddings and patch-text similarity, enhancing object-centered perspective. To compute the object presence prior P , we take an entire input image \mathcal{I} and compute likelihood for each class i as $P(i) = \{t_{\text{CLIP}}^i\}_{i=1}^C v_{\text{CLIP}}$, where the visual embedding vector $v_{\text{CLIP}} = \mathcal{F}_{\text{CLIP}}^v(\mathcal{I}) \in \mathbb{R}^d$ is derived from the ViT [CLS] token. The object presence prior is used in the following sections to enhance object-level context.

Object-Guided Text Embedding Adjustment. We adjust text embeddings $\{t_{\text{CLIP}}^i\}_{i=1}^C$ to embed object-specific contextual semantics, as shown in Fig. 5. To prevent object parts from being assigned to ambiguous classes, we hierarchically cluster text embeddings based on CLIP semantic distance, forming groups of similar embeddings

Table 1. Quantitative results with state-of-the-art unsupervised open-vocabulary semantic segmentation models on eight datasets.

Model	Supporting Dataset	Extra-Training	Fair	V21	PC60	C-Obj	V20	PC59	C-Stf	City	ADE	Avg.	
GroupViT [49]	CVPR'22	CC12M+RedCaps	✓	✗	50.4	18.7	27.5	79.7	23.4	15.3	11.1	9.2	29.4
TCL [9]	CVPR'23	CC3M+CC12M	✓	✗	55.0	30.4	31.6	83.2	33.9	22.4	24.0	17.1	37.2
CoDe [46]	CVPR'24	CC3M+RedCaps	✓	✗	57.5	30.5	32.3	-	-	23.9	28.9	17.7	-
CLIP-DINOiser [47]	ECCV'24	ImageNet1k	✓	✗	62.1	32.4	34.8	80.9	35.9	24.6	31.7	20.0	40.3
ReCo [40]	NeurIPS'22	ImageNet1k	✗	✗	25.1	19.9	15.7	57.7	22.3	14.8	21.6	11.2	23.5
FOSSIL [3]	WACV'24	COCO Captions	✗	✗	-	-	-	-	35.8	24.8	23.2	18.8	-
FreeDa [4]	CVPR'24	COCO Captions	✗	✗	-	-	-	85.6	43.1	27.8	36.7	22.4	-
CLIP [34]	ICML'21	✗	✗	✓	18.6	7.8	6.5	49.1	11.2	7.2	6.7	3.2	13.8
MaskCLIP [53]	ECCV'22	✗	✗	✓	38.3	23.6	20.6	74.9	26.4	16.4	12.6	9.8	27.9
GEM [6]	CVPR'24	✗	✗	✓	46.2	-	-	-	32.6	-	-	15.7	-
CaR [42]	CVPR'24	✗	✗	✓	48.6	13.6	15.4	73.7	18.4	-	-	5.4	-
PnP-OVSS [42]	CVPR'24	✗	✗	✓	-	-	36.2	51.3	28.0	17.9	-	14.2	-
CLIPtrase [39]	ECCV'24	✗	✗	✓	50.9	29.9	43.6	81.0	33.8	22.8	21.3	16.4	32.7
ClearCLIP [24]	ECCV'24	✗	✗	✓	51.8	32.6	33.0	80.9	35.9	23.9	30.0	16.7	38.1
SCLIP [43]	ECCV'24	✗	✗	✓	59.1	30.4	30.5	80.4	34.1	22.4	32.2	16.1	38.2
LaVG [20]	ECCV'24	✗	✗	✓	62.1	31.6	34.2	82.5	34.7	23.2	26.2	15.8	38.8
ProxyCLIP [25]	ECCV'24	✗	✗	✓	59.1	35.2	36.2	78.2	38.8	26.2	38.1	19.6	41.4
NACLIP [16]	WACV'25	✗	✗	✓	58.9	32.2	33.2	79.7	35.2	23.3	35.5	17.4	39.4
CASS		✗	✗	✓	65.8	36.7	37.8	87.8	40.2	26.7	39.4	20.4	44.4

$\mathcal{T}_g = \{t_{\text{CLIP}}^i \mid i \in I_g\}$, where \mathcal{T}_g is a subset of entire text embeddings $\{t_{\text{CLIP}}^i\}_{i=1}^C$ with index set I_g . Further details about this clustering process are provided in the supplementary materials. Within \mathcal{T}_g , we identify the object most likely to appear in the image using object presence prior P , formulated as $i^* = \arg \max_{i \in I_g} P(i)$. This facilitates refining the text embedding vector $t_{\text{CLIP}}^{i^*}$ to better represent object-contextual semantics. We note that patch-wise visual feature $F_{\text{CLIP}} \in \mathbb{R}^{N \times d}$ contains object-specific semantic vectors that can guide $t_{\text{CLIP}}^{i^*}$ accordingly. Thus, we compute cosine similarity between F_{CLIP} and $t_{\text{CLIP}}^{i^*}$ and select top- n object-specific image vector denoted as $\{f_i\}_{i=1}^n := \text{Concat}[f_1, \dots, f_n] \in \mathbb{R}^{n \times d}$. To define a targeted direction, we compute the average of $\{f_i\}_{i=1}^n$ as $\mu_n \in \mathbb{R}^d$, and guide selected text embedding $t_{\text{CLIP}}^{i^*}$ towards μ_n as

$$\tilde{t}_{\text{CLIP}}^{i^*} = (1 - \alpha) \cdot t_{\text{CLIP}}^{i^*} + \alpha \cdot \mu_n, \quad (8)$$

where α controls the degree of alignment with μ_n . The adjusted text embedding $\tilde{t}_{\text{CLIP}}^{i^*}$ replaces the original text embedding t_{CLIP}^i in the set $\{t_{\text{CLIP}}^i\}_{i=1}^C$, which is then used to compute the patch-text similarity logit \hat{S} in Eq. (4).

Object Perspective Patch-Text Similarity. We integrate the object presence prior with patch-text similarity \hat{S} from Eq. (4) to produce a segmentation map from an object-perspective view. Unlike Barsellotti *et al.* [4], which computes likelihood from an image window $\hat{\mathcal{I}}$, our approach derives similarity from the full image \mathcal{I} , enabling richer object-contextual understanding at the broader level. Thus, we refine the patch-text similarity \hat{S} from Eq. (4) to obtain the final patch-text similarity \hat{S}^* , computed as

$$\hat{S}^* = (1 - \gamma) \cdot \hat{S} + \gamma \cdot \{t_{\text{CLIP}}^i\}_{i=1}^C v_{\text{CLIP}}, \quad (9)$$

where γ controls the balance between \hat{S} and object presence prior. This enables the final segmentation map to capture object-level details, enabling precise, object-aware segmentation with accurate class assignments.

4. Experiments

We first describe the experimental settings, including implementation details, datasets, and evaluation metrics (Sec. 4.1). We then present quantitative and qualitative evaluation results (Sec. 4.2) and demonstrate ablation studies to assess each proposed component (Sec. 4.3). Additional experiment results are provided in the supplementary material.

4.1. Experimental Settings

Implementation Details. Similar to existing training-free approaches [16, 20, 25, 39, 43], we employ CLIP ViT-B/16 [34] as our VLM and DINO ViT-B/8 [8] as our VFM, both kept frozen to preserve a fully *training-free* design. For fair comparisons with prior work, input images are matched with the shorter side set to 336 pixels (or 560 pixels for the higher-resolution Cityscapes dataset), and sliding window inference is applied with a 224×224 window and a stride of 112 to achieve efficient evaluation coverage. Further details are provided in the supplementary material.

Datasets. Our primary datasets include PASCAL VOC 2012 [15], PASCAL Context [32], and COCO [7], each evaluated with and without a background class. We refer to the versions with a background class as V21, PC60, and C-Obj, and those without as V20, PC59, and C-Stf. We also report results on the ADE20K (ADE) [52] and Cityscapes (City) [13] datasets. These datasets contain 21, 60, 81, 20, 59, 171, 150, and 19 classes, respectively.

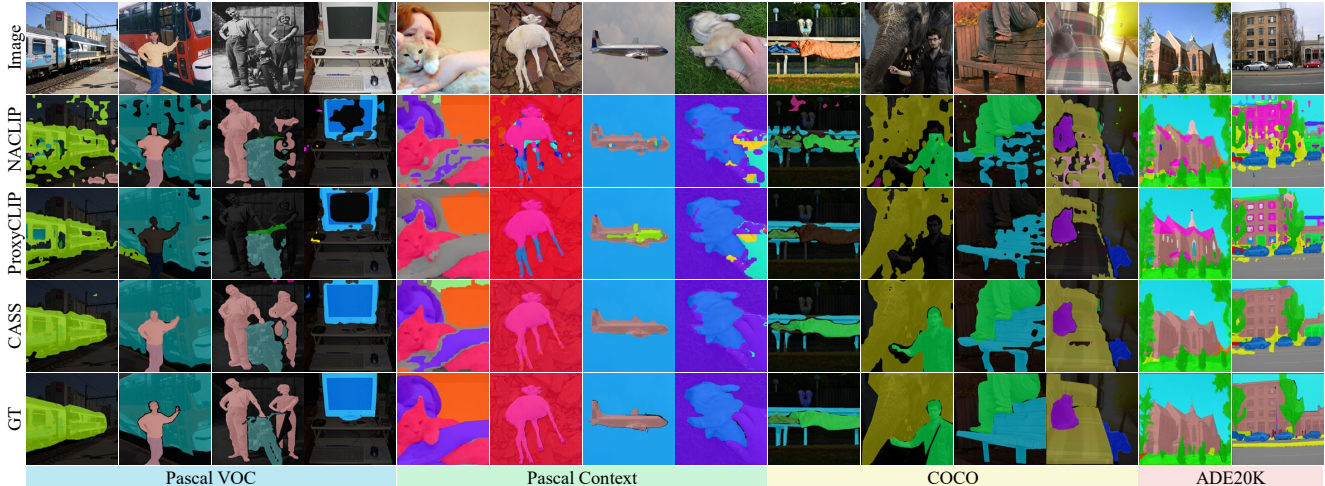


Figure 6. Qualitative comparison across the Pascal VOC [15], Pascal Context [32], COCO [7], and ADE20K [52] datasets using CLIP ViT-B/16 [34], evaluating previous state-of-the-art training-free OVSS methods, including NAACLIP [16], ProxyCLIP [25], and ours.

4.2. Evaluation Results

We evaluate the proposed model against existing training-free OVSS methods quantitatively and qualitatively. For fair comparisons, we refrain from using the mask refinement (e.g., PAMR [1] or DenseCRF [22]) and reproduce the results from [25], with a window size of 224×224 to match the baselines. We mainly report the mean Intersection over Union (mIoU) metric to evaluate our model. Additionally, we incorporate average pixel accuracy (pAcc) to provide more comprehensive evaluations.

Quantitative Evaluation: mIoU. Table 1 presents the main results in mIoU, where all results are obtained using CLIP ViT-B/16 as the backbone model for fair comparisons. To demonstrate the strengths of our model, we also include methods that use supporting datasets (i.e., retrieving additional datasets during inference) or additional training (models evaluated under the same setting as ours are indicated with \checkmark in the “Fair” column). Our model, CASS, performs favorably against the state-of-the-art methods, with an average gain of 3.0 mIoU point across eight datasets. Notably, for the V20, CASS achieves a performance gain of 5.3 mIoU point over the second-best model. Further, CASS outperforms CLIP-DINOiser [47] (which also leverages DINO with extra data and training) by 4.1 mIoU point.

Quantitative Evaluation: pAcc. Table 2 shows the results of pAcc on recent state-of-the-art models evaluated under the same settings. Our CASS outperforms the second-highest model by 2.3 pAcc point and exceeds one of the most recent papers, CLIPtrase [39], by 9.9 pAcc point. Our model consistently performs better than existing methods on mIoU and pAcc by effectively capturing object-level context, resulting in more accurate object masking.

Qualitative Analysis. Fig. 6 provides a qualitative comparison with recent state-of-the-art models [16, 25]. Existing

Table 2. Quantitative results using average pixel accuracy.

Model	V21	PC60	C-Obj	V20	PC59	C-Stf	City	ADE	Avg.
CLIPtrase [39]	78.6	52.1	50.1	89.7	58.9	38.9	63.4	38.6	59.1
LaVG [20]	89.3	48.7	74.8	91.1	58.9	39.1	68.5	37.0	63.4
SCLIP [43]	87.6	49.2	74.3	91.0	58.3	38.4	72.7	38.7	63.8
ProxyCLIP [25]	86.6	52.0	75.9	88.4	63.4	43.4	74.9	49.1	66.7
NAACLIP [16]	87.1	51.2	75.3	89.2	59.8	39.3	71.7	45.2	64.9
CASS	90.1	55.6	76.0	93.9	65.0	43.6	78.2	49.4	69.0

methods often produce noisy segmentation maps and do not group object components correctly, such as wheels within a car or a person’s head or arm. Additionally, they often misclassify object parts into ambiguous classes (e.g., a motorcycle as a bicycle or an airplane as a car). In contrast, based on a deep understanding of object-level context, our CASS generates clean segmentation maps that accurately group all object components, including slender parts such as human arms or animal legs, into their respective object classes.

4.3. Ablation Study

We perform ablation studies to analyze the proposed method. We use the datasets representative of segmentation tasks for all experiments: V21, PC59, C-Stf, following [43]. Please refer to the supplementary material for the additional ablation studies including VFM backbones and feature type.

Effect of Spectral VFM Distillation. Table 3 shows the results of incorporating VFM (Exp.#3) with the vanilla setting (Exp.#1), which directly uses the output from Eq. (4). In Exp.#3, A_{VFM} and A_{CLIP} are aggregated in a straightforward head-wise manner, without any additional processing to A_{VFM} . Simply leveraging A_{VFM} leads to a performance gain compared to the vanilla setting. Exp.#4 to Exp.#6 validate the effectiveness of the proposed components (see Sec. 3.2). Exp.#4 demonstrates the aggregation of A_{VFM} and A_{CLIP} using a complementary spectral graph matching (GM) procedure. Exp.#5, denoted as LR, presents the results with only the low-rank approximation applied to

Table 3. Ablation results showing the impact of our components on the performance across V21 [15], PC59 [32], and C-Stf [7]. The abbreviations in the table are noted in Sec. 4.3.

Exp. #	A_{VFM}	GM	LR	DE	OPS	OTA	Dataset		
							V21	PC59	C-Stf
1							58.9	35.3	23.4
2					✓	✓	59.2	36.5	24.0
3	✓						62.5	36.9	24.5
4	✓	✓					63.2	38.0	25.4
5	✓	✓	✓				64.5	38.6	25.7
6	✓	✓	✓	✓			64.8	39.1	25.9
7	✓	✓	✓	✓	✓		65.0	39.6	26.4
8	✓	✓	✓	✓	✓	✓	65.8	40.2	26.7

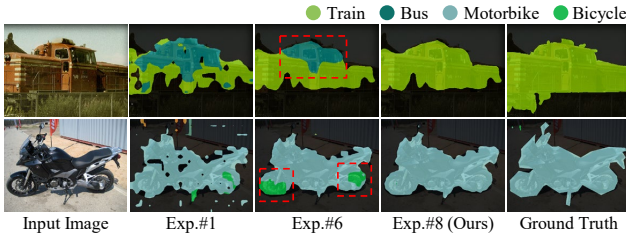


Figure 7. Qualitative ablation of our method. Exp.# refers to the experiment in Table 3. As additional components of our proposed method are incorporated, the segmentation map exhibits greater refinement and more effectively captures object-level context.

A_{VFM} , while Exp.#6 shows the results with both the low-rank approximation and Dynamic Eigenscaling (DE) applied, as defined in Eq. (6). Notably, Exp.#6 shows significant performance gain over simply integrating VFM knowledge (Exp.#3), demonstrating the effectiveness of graph matching and low-rank approximation in capturing object-level context. Fig. 3 qualitatively visualizes the attention map, with the left, middle, and right columns corresponding to Exp.#3, Exp.#4, and Exp.#6, respectively. We observe that integrating proposed low-rank dynamic eigenscaling effectively reduces noise and emphasizes objects by highlighting objects with strong inter-object associations.

Effect of Object Presence Prior. We validate the effectiveness of the object presence prior-driven methods in Exp.#7 and Exp.#8 by examining each component: Object-Perspective Patch-Text Similarity (OPS) and Object-Guided Text Embedding Adjustment (OTA) (see Sec. 3.3). These results show that each component effectively improves performance, emphasizing object-level context. Additionally, incorporating the object presence prior-driven methods on top of the vanilla setting, as shown in Exp.#2, clarifies the effectiveness of the proposed method.

Qualitative Ablations. Fig. 7 shows the segmentation maps for the vanilla setting (Exp.#1), after applying spectral VFM distillation (Exp.#6), and with all proposed components applied (Exp.#8). While Exp.#6 improves object masking compared to Exp.#1, it often misses parts of objects (highlighted by the red dotted line). In contrast, incorporating all proposed components (Exp.#8) consolidates

Table 4. Ablation results on different CLIP backbones.

Model	V21		PC59		C-Stf		Avg. mIoU	Avg. pAcc
	mIoU	pAcc	mIoU	pAcc	mIoU	pAcc		
ViT-B/32	SCLIP [43]	50.6	81.0	28.7	49.6	20.0	33.4	54.7
	LaVG [20]	54.8	84.4	29.0	50.1	20.5	33.7	56.1
	ProxyCLIP [25]	57.9	85.6	35.2	59.7	23.6	40.2	61.8
	NACLIP [16]	51.1	82.8	32.4	56.8	21.2	37.1	58.9
	CASS	58.2	86.2	36.5	61.0	24.4	40.8	62.7
ViT-L/14	SCLIP [43]	44.4	78.1	25.2	46.6	17.6	29.6	51.4
	LaVG [20]	51.5	84.1	27.5	50.3	19.4	32.3	55.6
	ProxyCLIP [25]	59.8	85.7	38.3	61.0	26.2	43.5	63.4
	NACLIP [16]	52.2	83.1	32.1	52.8	21.4	35.7	57.2
	CASS	62.1	88.0	39.1	62.1	26.3	43.4	64.5

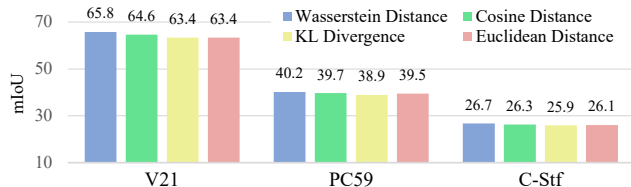


Figure 8. Performance evaluation of different distance metrics used in graph matching and graph distillation.

objects into single entities, effectively capturing object-level context in the segmentation mask.

Different CLIP Backbones. Table 4 shows results on different CLIP backbones, ViT-B/32 and ViT-L/14. Our CASS performs favorably across various backbones, consistently outperforming existing methods in mIoU and pAcc. These results demonstrate the effectiveness and robustness of our method across different backbone architectures.

Distance Metric for Graph Matching. We evaluate different distance metrics \mathcal{D}_W used in Sec. 3.2.1, including Wasserstein Distance, Cosine Distance, KL Divergence, and Euclidean Distance. As shown in Fig. 8, the Wasserstein Distance shows the best results as it provides an intuitive measure of the overall shape of sorted eigenvalue distributions. While we use Wasserstein Distance due to its performance, the other well-known metrics exhibited comparable results, demonstrating the robustness of our method in terms of the choice of a distance metric and further supporting the effectiveness of our proposed approach.

5. Conclusion

In this work, we present CASS, a training-free approach for open-vocabulary semantic segmentation that integrates object-level context into CLIP. By distilling object-aware structural information from VFM into CLIP’s attention, CASS effectively enhances intra-object coherence, ensuring that each object is consistently represented as a unified semantic entity. Additionally, we leverage an object presence prior knowledge to adjust text embeddings and refine object class assignments, aligning them with object-specific semantic targets in the image. Consequently, CASS addresses key limitations of training-free OVSS in accurately grouping object components and assigning semantic classes without extra training or additional labeled data, making it a robust solution across diverse datasets and visual contexts.

References

- [1] Nikita Araslanov and Stefan Roth. Single-stage semantic segmentation from image labels. In *CVPR*, 2020. 7
- [2] Danny Barash and Matan Gavish. Optimal shrinkage of singular values under random data contamination. *NeurIPS*, 2017. 5
- [3] Luca Barsellotti, Roberto Amoroso, Lorenzo Baraldi, and Rita Cucchiara. Fossil: Free open-vocabulary semantic segmentation through synthetic references retrieval. In *WACV*, 2024. 2, 6
- [4] Luca Barsellotti, Roberto Amoroso, Marcella Cornia, Lorenzo Baraldi, and Rita Cucchiara. Training-free open-vocabulary segmentation with offline diffusion-augmented prototype generation. In *CVPR*, 2024. 2, 6
- [5] Toby Boas, Aritra Dutta, Xin Li, Kathryn P Mercier, and Eric Niderman. Shrinkage function and its applications in matrix approximation. *arXiv preprint arXiv:1601.07600*, 2016. 5
- [6] Walid Bousellham, Felix Petersen, Vittorio Ferrari, and Hilde Kuehne. Grounding everything: Emerging localization properties in vision-language transformers. In *CVPR*, 2024. 6
- [7] Holger Caesar, Jasper Uijlings, and Vittorio Ferrari. COCO-Stuff: Thing and Stuff Classes in Context. In *CVPR*, 2018. 6, 7, 8
- [8] Mathilde Caron, Hugo Touvron, Ishan Misra, Hervé Jégou, Julien Mairal, Piotr Bojanowski, and Armand Joulin. Emerging Properties in Self-Supervised Vision Transformers. In *ICCV*, 2021. 2, 4, 6
- [9] Junbum Cha, Jonghwan Mun, and Byungseok Roh. Learning To Generate Text-Grounded Mask for Open-World Semantic Segmentation From Only Image-Text Pairs. In *CVPR*, 2023. 1, 6
- [10] Liang-Chieh Chen, Yukun Zhu, George Papandreou, Florian Schroff, and Hartwig Adam. Encoder-decoder with atrous separable convolution for semantic image segmentation. In *ECCV*, 2018. 1, 3
- [11] Seokju Cho, Heeseong Shin, Sunghwan Hong, Anurag Arnab, Paul Hongsuck Seo, and Seungryong Kim. Cat-seg: Cost aggregation for open-vocabulary semantic segmentation. In *CVPR*, 2024. 1
- [12] Fan RK Chung. *Spectral graph theory*. American Mathematical Soc., 1997. 4
- [13] Marius Cordts, Mohamed Omran, Sebastian Ramos, Timo Rehfeld, Markus Enzweiler, Rodrigo Benenson, Uwe Franke, Stefan Roth, and Bernt Schiele. The Cityscapes Dataset for Semantic Urban Scene Understanding. In *CVPR*, 2016. 6
- [14] Alexey Dosovitskiy, Lucas Beyer, Alexander Kolesnikov, Dirk Weissenborn, Xiaohua Zhai, Thomas Unterthiner, Mostafa Dehghani, Matthias Minderer, Georg Heigold, Sylvain Gelly, Jakob Uszkoreit, and Neil Houlsby. An Image is Worth 16x16 Words: Transformers for Image Recognition at Scale. In *ICLR*, 2021. 2
- [15] M. Everingham, L. Van Gool, C. K. I. Williams, J. Winn, and A. Zisserman. The PASCAL Visual Object Classes Challenge 2012 (VOC2012) Results, 2012. 6, 7, 8
- [16] Sina Hajimiri, Ismail Ben Ayed, and Jose Dolz. Pay attention to your neighbours: Training-free open-vocabulary semantic segmentation. In *WACV*, 2025. 1, 2, 3, 6, 7, 8
- [17] Mark Hamilton, Zhoutong Zhang, Bharath Hariharan, Noah Snavely, and William T Freeman. Unsupervised semantic segmentation by distilling feature correspondences. *arXiv preprint arXiv:2203.08414*, 2022. 2, 3
- [18] Ali Hatamizadeh, Yucheng Tang, Vishwesh Nath, Dong Yang, Andriy Myronenko, Bennett Landman, Holger R Roth, and Daguang Xu. Unetr: Transformers for 3d medical image segmentation. In *CVPR*, 2022. 1, 3
- [19] Ruixiang Jiang, Lingbo Liu, and Changwen Chen. Clip-count: Towards text-guided zero-shot object counting. In *ACM Multimedia*, 2023. 2, 5
- [20] Dahyun Kang and Minsu Cho. In defense of lazy visual grounding for open-vocabulary semantic segmentation. In *ECCV*, 2024. 2, 6, 7, 8
- [21] Chanyoung Kim, Woojung Han, Dayun Ju, and Seong Jae Hwang. Eagle: Eigen aggregation learning for object-centric unsupervised semantic segmentation. In *CVPR*, 2024. 2, 3
- [22] Philipp Krähenbühl and Vladlen Koltun. Efficient Inference in Fully Connected CRFs with Gaussian Edge Potentials. In *NeurIPS*, 2011. 7
- [23] Harold W Kuhn. The hungarian method for the assignment problem. *Naval research logistics quarterly*, 1955. 4
- [24] Mengcheng Lan, Chaofeng Chen, Yiping Ke, Xinjiang Wang, Litong Feng, and Wayne Zhang. Clearclip: Decomposing clip representations for dense vision-language inference. In *ECCV*, 2024. 1, 6
- [25] Mengcheng Lan, Chaofeng Chen, Yiping Ke, Xinjiang Wang, Litong Feng, and Wayne Zhang. Proxyclick: Proxy attention improves clip for open-vocabulary segmentation. In *ECCV*, 2024. 1, 2, 3, 6, 7, 8
- [26] Yi Li, Hualiang Wang, Yiqun Duan, and Xiaomeng Li. Clip surgery for better explainability with enhancement in open-vocabulary tasks. *arXiv preprint arXiv:2304.05653*, 2023. 2
- [27] Yiran Li, Junpeng Wang, Xin Dai, Liang Wang, Chinchia Michael Yeh, Yan Zheng, Wei Zhang, and Kwan-Liu Ma. How does attention work in vision transformers? a visual analytics attempt. *IEEE Transactions on Visualization and Computer Graphics*, 2023. 4
- [28] Feng Liang, Bichen Wu, Xiaoliang Dai, Kunpeng Li, Yanan Zhao, Hang Zhang, Peizhao Zhang, Peter Vajda, and Diana Marculescu. Open-vocabulary semantic segmentation with mask-adapted clip. In *CVPR*, 2023. 1
- [29] Yunyao Mao, Jiajun Deng, Wengang Zhou, Li Li, Yao Fang, and Houqiang Li. Clip4hoi: towards adapting clip for practical zero-shot hoi detection. *NeurIPS*, 2023. 2, 5
- [30] Octave Mariotti, Oisín Mac Aodha, and Hakan Bilen. Improving semantic correspondence with viewpoint-guided spherical maps. In *CVPR*, 2024. 2
- [31] Luke Melas-Kyriazi, Christian Rupprecht, Iro Laina, and Andrea Vedaldi. Deep spectral methods: A surprisingly strong baseline for unsupervised semantic segmentation and localization. In *CVPR*, 2022. 2, 3

- [32] Roozbeh Mottaghi, Xianjie Chen, Xiaobai Liu, Nam-Gyu Cho, Seong-Whan Lee, Sanja Fidler, Raquel Urtasun, and Alan Yuille. The Role of Context for Object Detection and Semantic Segmentation in the Wild. In *CVPR*, 2014. 6, 7, 8
- [33] Maxime Oquab, Timothée Darcet, Théo Moutakanni, Huy Vo, Marc Szafraniec, Vasil Khalidov, Pierre Fernandez, Daniel Haziza, Francisco Massa, Alaaeldin El-Nouby, et al. Dinov2: Learning robust visual features without supervision. *arXiv preprint arXiv:2304.07193*, 2023. 2
- [34] Alec Radford, Jong Wook Kim, Chris Hallacy, Aditya Ramesh, Gabriel Goh, Sandhini Agarwal, Girish Sastry, Amanda Askell, Pamela Mishkin, Jack Clark, et al. Learning Transferable Visual Models From Natural Language Supervision. In *ICML*, 2021. 1, 2, 3, 5, 6, 7
- [35] Olaf Ronneberger, Philipp Fischer, and Thomas Brox. U-net: Convolutional networks for biomedical image segmentation. In *MICCAI*, 2015. 1, 3
- [36] Maximilian Seitzer, Max Horn, Andrii Zadaianchuk, Dominik Zietlow, Tianjun Xiao, Carl-Johann Simon-Gabriel, Tong He, Zheng Zhang, Bernhard Schölkopf, Thomas Brox, and Francesco Locatello. Bridging the gap to real-world object-centric learning. In *ICLR*, 2023. 3
- [37] Hyun Seok Seong, WonJun Moon, SuBeen Lee, and Jae-Pil Heo. Leveraging hidden positives for unsupervised semantic segmentation. In *CVPR*, 2023. 2, 3
- [38] Xiangheng Shan, Dongyue Wu, Guilin Zhu, Yuanjie Shao, Nong Sang, and Changxin Gao. Open-vocabulary semantic segmentation with image embedding balancing. In *CVPR*, 2024. 1
- [39] Tong Shao, Zhuotao Tian, Hang Zhao, and Jingyong Su. Explore the potential of clip for training-free open vocabulary semantic segmentation. In *ECCV*, 2024. 3, 6, 7
- [40] Gyungin Shin, Weidi Xie, and Samuel Albanie. ReCo: Retrieve and Co-segment for Zero-shot Transfer. In *NeurIPS*, 2022. 6
- [41] Oriane Siméoni, Gilles Puy, Huy V Vo, Simon Roburin, Spyros Gidaris, Andrei Bursuc, Patrick Pérez, Renaud Marlet, and Jean Ponce. Localizing objects with self-supervised transformers and no labels. In *BMVC*, 2021. 2, 3
- [42] Shuyang Sun, Runjia Li, Philip Torr, Xiuye Gu, and Siyang Li. Clip as rnn: Segment countless visual concepts without training endeavor. In *CVPR*, 2024. 2, 6
- [43] Feng Wang, Jieru Mei, and Alan Yuille. Sclip: Rethinking self-attention for dense vision-language inference. In *ECCV*, 2024. 1, 2, 3, 6, 7, 8
- [44] Xudong Wang, Rohit Girdhar, Stella X Yu, and Ishan Misra. Cut and Learn for Unsupervised Object Detection and Instance Segmentation. In *CVPR*, 2023. 2
- [45] Xin Wen, Bingchen Zhao, Anlin Zheng, Xiangyu Zhang, and Xiaojuan Qi. Self-supervised visual representation learning with semantic grouping. *NeurIPS*, 2022. 3
- [46] Ji-Jia Wu, Andy Chia-Hao Chang, Chieh-Yu Chuang, Chun-Pei Chen, Yu-Lun Liu, Min-Hung Chen, Hou-Ning Hu, Yung-Yu Chuang, and Yen-Yu Lin. Image-text co-decomposition for text-supervised semantic segmentation. In *CVPR*, 2024. 6
- [47] Monika Wysoczańska, Oriane Siméoni, Michaël Ramamonjisoa, Andrei Bursuc, Tomasz Trzcíński, and Patrick Pérez. Clip-dinoiser: Teaching clip a few dino tricks. *arXiv preprint arXiv:2312.12359*, 2023. 6, 7
- [48] Bin Xie, Jiale Cao, Jin Xie, Fahad Shahbaz Khan, and Yanwei Pang. Sed: A simple encoder-decoder for open-vocabulary semantic segmentation. In *CVPR*, 2024. 1
- [49] Jiarui Xu, Shalini De Mello, Sifei Liu, Wonmin Byeon, Thomas Breuel, Jan Kautz, and Xiaolong Wang. GroupViT: Semantic Segmentation Emerges From Text Supervision. In *CVPR*, 2022. 1, 6
- [50] Jiarui Xu, Sifei Liu, Arash Vahdat, Wonmin Byeon, Xiaolong Wang, and Shalini De Mello. Open-vocabulary panoptic segmentation with text-to-image diffusion models. In *CVPR*, 2023. 1
- [51] Mengde Xu, Zheng Zhang, Fangyun Wei, Han Hu, and Xiang Bai. Side adapter network for open-vocabulary semantic segmentation. In *CVPR*, 2023. 1
- [52] Bolei Zhou, Hang Zhao, Xavier Puig, Tete Xiao, Sanja Fidler, Adela Barriuso, and Antonio Torralba. Semantic Understanding of Scenes Through the ADE20K Dataset. *IJCV*, 2019. 6, 7
- [53] Chong Zhou, Chen Change Loy, and Bo Dai. Extract Free Dense Labels from CLIP. In *ECCV*, 2022. 1, 2, 6
- [54] Lianghui Zhu, Yingyue Li, Jiemin Fang, Yan Liu, Hao Xin, Wenyu Liu, and Xinggang Wang. Weaktr: Exploring plain vision transformer for weakly-supervised semantic segmentation. *arXiv preprint arXiv:2304.01184*, 2023. 4